Different routes into the glass state for soft thermo-sensitive colloids

Rodrigo Rivas-Barbosa,[a] Edilio Lázaro-Lázaro,[b] Patricia Mendoza-Mendez,[c] Tim Still,[d] Valeria Piazza,[e] Pedro E. Ramırez-González,[f] Magdaleno Medina-Noyola,[c] and Marco Laurati*[a]

[a] *División de Ciencias e Ingenierías, Universidad de Guanajuato, Loma del Bosque 103, 37150 León, Mexico.*

[b] *Instituto de Física "Manuel Sandoval Vallarta", Universidad Autónoma de San Luis Potosí, Álvaro Obregón 64, 78000 San Luis Potosí, SLP, Mexico.*

[c] *Department of Chemical Engineering, Whitacre College of Engineering, Texas Tech University, Lubbock, Texas 79409-3121, USA.*

[d] *Department of Physics and Astronomy, University of Pennsylvania, Philadelphia, Pennsylvania 19104, USA.*

[e] *Centro de Investigaciones en Óptica A.C., León, Mexico.*

[f] *CONACYT - Instituto de Física "Manuel Sandoval Vallarta", Universidad Autónoma de San Luis Potosí, Álvaro Obregón 64, 78000 San Luis Potosí, SLP, Mexico.*

We report an experimental and theoretical investigation of glass formation in soft thermo-sensitive colloids following two different routes: a gradual increase of the particle number density at constant temperature and an increase of the radius in a fixed volume at constant particle number density. Confocal microscopy experiments and the non-equilibrium self-consistent generalized Langevin equation (NE-SCGLE) theory consistently show that the two routes lead to a dynamically comparable state at sufficiently long aging times. However, experiments reveal the presence of moderate but persistent structural differences. Successive cycles of radius decrease and increase lead instead to a reproducible glass state, indicating a suitable route to obtain rejuvenation without using shear fields.

I. INTRODUCTION

Microgel colloids of poly-N-Isopropylacrilamide (PNIPAM) have attracted much interest in recent years as a model soft colloidal system which is sensitive to different stimuli, like temperature, pH, flow, or osmotic pressure [1]. Their softness can be tuned by the synthesis of the microgel and changes in the external stimuli [2–5]. Among the many applications of this system we find drug delivery, biosensing and photonics [1, 6–8]. On a more fundamental level, dispersions of PNIPAM colloids have been studied intensively as a model system to investigate crystallisation [9–14], glass formation [15–24], and jamming [9, 22, 23, 25–29]. Glass formation and jamming are solidification transitions induced by compression, which are typically observed for thermal or athermal systems, respectively. The glass transition is a dynamical arrest transition corresponding to the loss of ergodicity, while jamming is related to geometrical constraints which impede further compression, typically associated with close packing [30]. It has been recently suggested that depending on the particle size, the solidification transition in this system could be dominated by glassy or jamming physics [23, 26, 29], with the glass transition dominating when the particle size does not substantially exceed a few micrometers [23]. For the glass transition, it has been found that vitrification is shifted to larger effective volume fractions compared to hard spheres [18, 21, 28], however showing still the same entropic nature [31]. Additional fundamental differences are observed, for instance in the fragility [19], rheological response [21, 29, 32], and aging [20, 33–35].

The solid in this microgel system can be reached following two distinct routes. In the most investigated route, the transition to the solid state is induced from the fluid state at temperature $T \gtrsim 30$ °C through a rapid decrease in temperature below 25 °C. This route exploits the drastic increase of the radius of PNIPAM spheres below around 32 °C [1, 9, 36, 37], to obtain a strong and rapid volume fraction change, which quenches the system into the arrested state. In the second, much less explored case, the route to the arrested state corresponds to increasing the particle number density of the system while keeping the radius fixed (by keeping the temperature constant). This route can be only explored if crystallisation can be avoided [28], i.e. for sufficiently large polydispersity of the particles, typically more than 5% similar to hard spheres [38–40].

The two routes lead to an arrested state in a rather different way: in the radius increase route, the initial structure of the sample is that of a fluid and the sudden swelling of the particles leads to arrest abruptly; one can speculate that the rearrangement of the fluid structure is at least partially frustrated by the rapid swelling of the particles. On the other hand, the gradual increase in particle number density at constant radius necessarily involves restructuring of the dispersion to allow a higher degree of packing of the particles. One might therefore wonder whether the two paths lead to comparable arrested states, a question which has not been addressed to date and is relevant to understand glass formation in thermosensitive colloids.

In this report we compare the particle number density and radius variation routes to achieve an arrested state in PNIPAM microgel dispersions. The size of our particles is of the order of the micrometer and therefore glassy physics should be still dominant in this regime [23], however we cannot entirely exclude some contributions arising from jamming effects. Using confocal microscopy we determine and compare the structure and dynamics of

arrested states obtained along a process in which a solid initially formed by compression is first melted by reducing the particle radius through a temperature increase, and successively reformed increasing the particle radius through a temperature decrease. We confront the experimental results to comparable protocols obtained through the non-equilibrium self-consistent generalized Langevin equation (NE-SCGLE) theory of the glass transition, obtaining remarkable qualitative agreement. This supports the interpretation of the fluid-solid transition in our system in terms of the glass transition. We find that the glass formed through the increase of particle number density is structurally more ordered than the glass reformed through the radius variation process, even when comparable aging times are considered. At the same time, glasses formed by consecutive temperature variation processes are reproducible, indicating a suitable route to rejuvenation .

II. MATERIALS AND METHODS

A. Samples

We used PNIPAM colloids synthesized following the route described in previous work [41]. The particle size and polydispersity in dilute conditions at temperature T = 25 °C, $R = 0.9 \pm 0.1$ µm was determined by Dynamic Light Scattering. The T-dependence of the particle size in dilute conditions was characterized previously [41] and was used to determine the value of R at the different temperatures studied. In the range of investigated temperatures $25 < T < 30$ °C the T-dependence of R is approximately linear as estimated by fitting the data in Ref.[41]. Using the slope obtained from the fit of the data in Ref.[41], we determined the radius at different temperatures T as $R(T) = R(T = 25°C) - aT$, where $a = 24.337\,\mu$m/°C. Data are reported in Tab.I. The particles were labeled with carboxytetramethylrhodamine (TAMRA) dye. Dispersions of PNIPAM colloids at different concentrations were prepared in deionized water starting from a low volume fraction solution, the particle number density of which was determined with confocal microscopy, as detailed in the next section. No salt was added to the samples and therefore the system carries a certain amount of charge[42]. In order to disperse the particles uniformly, the solution was mixed using a magnetic stirrer. Increasingly larger concentrations were obtained in multiple steps by slowly drying the original dispersion in a vacuum oven at room temperature. By means of the very slow drying process we avoid the occurrence of concentration gradients, as later verified by imaging. Samples were prepared in vials for confocal microscopy. The highest concentration sample was used for the successive radius variation experiments, where the temperature was used to control the variation of the particle radius and therefore ϕ.

TABLE I. Top: Particle radius as a function of temperature, as determined by using the T-dependence of R reported in Ref.[41]. In addition, the value of the area fraction ϕ_A for sample S6 (see table below) is reported for the different temperatures, as estimated through R and the average number of particles per image plane $\langle n_p \rangle$. Bottom: Samples obtained at T = 25 °C progressively increasing concentration: corresponding average number of particles per image plane $\langle n_p \rangle$ and area fraction ϕ_A

T (°C)	2R (μm)	$\langle n_p \rangle$	ϕ_A
25	1.80	1179	0.68
26	1.775	1194	0.67
27	1.75	1218	0.66
28	1.73	1254	0.65
29	1.70	1257	0.64
30	1.68	1258	0.63

Sample	$\langle n_p \rangle$	ϕ_A
S1	403	0.23
S2	500	0.29
S3	681	0.39
S4	922	0.53
S5	1137	0.65
S6	1196	0.69

B. Confocal Microscopy

Confocal microscopy experiments were performed on a Zeiss LSM 710 confocal microscope, using a 63x oil immersion objective (NA = 1.46) and a 546nm wavelength HeNe laser as illumination source. For the investigation of the structural arrangement of the particles we acquired 10 independent time series of 200 in-plane images each, with an image size of 512×512 pixels, corresponding to an area A of 66.56×66.56 μm^2 (0.13 μm/pixel). The total of 2000 images was used to obtain statistical averaging of the structural properties. For the determination of particle dynamics we acquired 5 independent series of 2000 images each, with an image size of 256×256 pixels (Area A 33.28×33.28 μm^2), at a frame rate of approximately 8.3 fps. The image size in this case was reduced in order to avoid that particles perform large excursions between two consecutive images, which would complicate the determination of trajectories using particle tracking. Particle coordinates and trajectories were extracted from the images using standard analysis routines [43]. Temperature was controlled via a combination of a heating plate and an incubation chamber (Peckon), and measured with a thermocouple thermometer positioned on the sample. The accuracy on the temperature setting was of ±0.1°C. The particle's area fraction ϕ_A was determined as $\phi_A = n_p \pi R^2/A$, with R the radius of the particles at 25 °C and n_p the average number of particles encountered in the 2000 images used for structural characterization. The investigated samples and corresponding area fractions obtained through the concentration procedure are

listed in Tab.I. For the investigated ϕ_A we did not observe a significant change in the particle radius R as a function of ϕ_A.

C. NE-SCGLE theory

The NE-SCGLE theory describes the overall evolution of the structural and dynamical properties of a glass-forming liquid as a function of the waiting time t_w. The most general version of the NE-SCGLE theory [44] allows the calculation of the non-homogeneous evolution of a liquid from an initial state to the final stationary state. However, calculations using this general version are extremely demanding [44]. Affordable calculations can be performed under the assumption that the local density is approximately uniform. Under conditions of spatial uniformity, the NE-SCGLE theory determines that the time-evolution equation for the covariance (Eq. (2.11) of Ref. [45]) may be written as an equation for the non-equilibrium structure factor $S(k;t)$ which, for $t > 0$, reads

$$\frac{\partial S(k;t)}{\partial t} = -2k^2 D^0 b(t) \overline{n}^{(f)} \mathcal{E}^{(f)}(k) \left[S(k;t) - 1/\overline{n}\mathcal{E}^{(f)}(k) \right]. \tag{1}$$

In this equation the function $\mathcal{E}^{(f)}(k) = \mathcal{E}(k;\overline{n},T^{(f)})$ is the Fourier transform (FT) of the functional derivative:

$$\mathcal{E}[\mid \mathbf{r} - \mathbf{r}' \mid ;n,T] \equiv [\delta\beta\mu[\mathbf{r};n]/\delta n(\mathbf{r}')] \tag{2}$$

evaluated at $n(\mathbf{r}) = \overline{n}$ and $T = T^{(f)}$. As discussed in Refs. [44, 45], this thermodynamic object embodies the information, which is assumed to be known, of the chemical equation of state, i.e., of the functional dependence of the electrochemical potential $\mu[\mathbf{r};n]$ on the number density profile $n(\mathbf{r})$.

The solution of this equation, for arbitrary initial conditions $S(k;t=0) = S^{(i)}(k)$, can be written as

$$S(k;t) = S^{(i)}(k) e^{-\alpha(k)u(t)} + [\overline{n}\mathcal{E}^{(f)}(k)]^{-1} \left(1 - e^{-\alpha(k)u(t)}\right), \tag{3}$$

with

$$\alpha(k) \equiv 2k^2 D^0 \overline{n} \mathcal{E}^{(f)}(k), \tag{4}$$

and with

$$u(t) \equiv \int_0^t b(t')dt'. \tag{5}$$

In the equations above, the time-evolving mobility $b(t)$ is defined as $b(t) \equiv D_L(t)/D^0$, with D^0 being the short-time self-diffusion coefficient and $D_L(t)$ the long-time self-diffusion coefficient at evolution time t. As explained in Refs. [44] and [45], the equation

$$b(t) = [1 + \int_0^\infty d\tau \Delta\zeta^*(\tau;t)]^{-1} \tag{6}$$

relates $b(t)$ with the time-evolving, τ-dependent friction coefficient $\Delta\zeta^*(\tau;t)$, which is given approximately by

$$\Delta\zeta^*(\tau;t) = \frac{D_0}{24\pi^3\overline{n}} \int d\mathbf{k}\ k^2 \left[\frac{S(k;t)-1}{S(k;t)}\right]^2 \times F(k,\tau;t) F_S(k,\tau;t). \tag{7}$$

Thus, the presence of $b(t)$ in Eq. (5) couples the formal solution for $S(k;t)$ in Eq. (3) with the solution of the non-equilibrium version of the SCGLE equations for the collective and self NE-ISFs $F(k,\tau;t)$ and $F_S(k,z;t)$. These equations are written, in terms of the Laplace transforms (LT) $F(k,z;t)$ and $F_S(k,\tau;t)$, as

$$F(k,z;t) = \frac{S(k;t)}{z + \frac{k^2 D^0 S^{-1}(k;t)}{1+\lambda(k)\ \Delta\zeta^*(z;t)}}, \tag{8}$$

and

$$F_S(k,z;t) = \frac{1}{z + \frac{k^2 D^0}{1+\lambda(k)\ \Delta\zeta^*(z;t)}}, \tag{9}$$

with $\lambda(k)$ being a phenomenological "interpolating function" [46], given by

$$\lambda(k) = 1/[1 + (k/k_c)^2], \tag{10}$$

with $k_c = 1.118 \times k_{max}(t)$, where $k_{max}(t)$ is the position of the main peak of $S(k;t)$. The simultaneous solution of Eqs. (1)-(9) above, constitute the NE-SCGLE description of the spontaneous evolution of the structure and dynamics of an *homogeneously* quenched liquid.

The theoretical model chosen for the molecular interactions is the well known Weeks-Chandler-Andersen soft-sphere potential [47, 48], which vanishes for $r \geq \sigma$, but which for $r \leq \sigma$ is given, in units of the thermal energy $k_B T = \beta^{-1}$, by

$$\beta u(r) = \epsilon \left[\left(\frac{\sigma}{r}\right)^{2\nu} - 2\left(\frac{\sigma}{r}\right)^{\nu} + 1 \right]. \tag{11}$$

The state space of this system is spanned by the volume fraction $\phi = \pi\overline{n}\sigma^3/6$ and the reduced temperature $T^* \equiv k_B T/\epsilon$. Note that different from the experiments, the volume fraction instead of the area fraction is used in the theoretical calculations.

III. RESULTS AND DISCUSSION

A. Vitrification by Variation of the Particle Number Density at Constant Radius

In this section we present results on the structure and dynamics of samples prepared at a constant radius R = 0.9 μm (by keeping T = 25 °C) and with increasingly larger particle number densities, corresponding to increasingly larger ϕ_A. Note that the samples were not

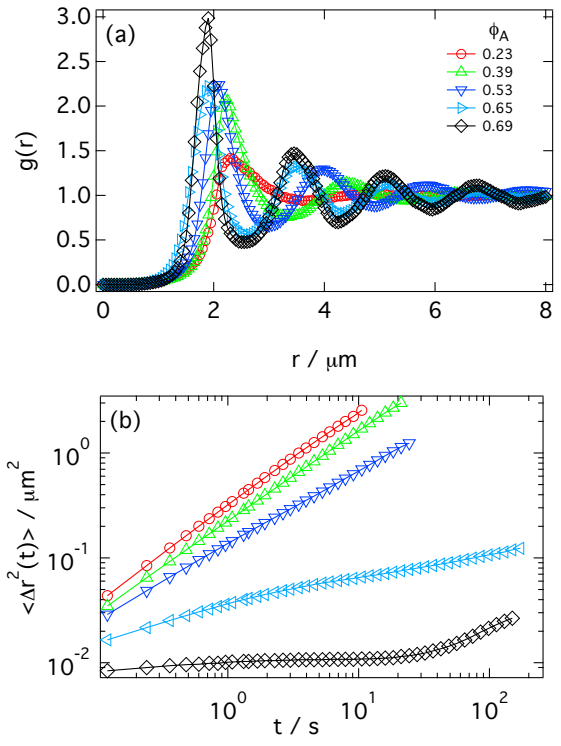

FIG. 1. (a) Radial distribution function $g(r)$ and (b) Mean square displacement $\langle \Delta r^2(t) \rangle$ obtained from experiments for samples with different area fraction ϕ_A (as indicated), measured at T = 25 °C.

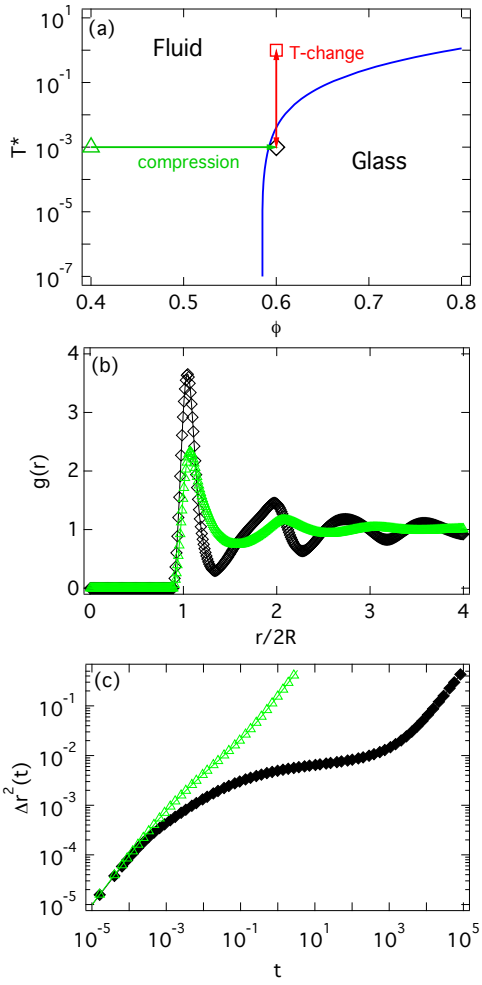

FIG. 2. (a) State diagram of the theoretical model system, indicating the vitrification boundary (blue solid line), the fluid state at $\phi = 0.4$, $T^* = 0.001$ (green triangle), the fluid state at $\phi = 0.6$, $T^* = 1.0$ (red square) and the glassy state at $\phi = 0.6$ and $T^* = 0.001$ (black diamond). The green arrow indicates the compression process, the red arrows the temperature change process. (b) Radial distribution function $g(r)$ and (c) Mean square displacement $\langle \Delta r^2(t) \rangle$ obtained from NE-SCGLE theory for samples with volume fraction $\phi = 0.40$ (triangles) and $\phi = 0.60$ (diamonds), at $T^* = 0.001$.

subjected to any kind of shear rejuvenation before measuring. Using the particle coordinates extracted from image series we calculated the 2D radial distribution functions of samples with different area fraction ϕ_A, starting from $\phi_A = 0.23$ (Fig.1a). We observe that with increasing ϕ_A the peaks of $g(r)$ progressively become larger and move to shorter distances, as a result of the increasingly smaller average inter-particle distance and the increased probability of contacts. The corresponding mean squared displacements (MSD) $\langle \Delta r^2(t) \rangle$ (Fig.1b) show the progressive slowing down of the dynamics. The initial diffusive behavior at the lowest concentrations ($\phi_A = 0.23$ and 0.39), with a diffusion constant that decreases from D = 0.069 μm^2 at $\phi_A = 0.23$ to D = 0.033 μm^2 at $\phi_A = 0.39$, becomes a sub-diffusive behavior at $\phi_A = 0.53$. The sub-diffusive dynamics become then particularly pronounced for $\phi_A = 0.65$. Finally, the sample with $\phi_A = 0.69$ shows the appearance of an extended plateau which indicates dynamical arrest, and an apparent increase at long times, which suggests a slow relaxation possibly due to activated processes [49]. The dynamics of the sample with $\phi_A = 0.69$ indicate the formation of a glass state, in agreement with previous results on a similar system [28]. During the preparation process, which consists in a very slow solvent evaporation, the sample ages and we can estimate an initial aging of $t_a \sim 10^4 t_B$, with $t_B \approx 26.7$ s the Brownian relaxation time, i.e. the time required by a colloidal particle to diffuse a distance equal to its diameter. We monitored the evolution of the structure and dynamics of the sample with increasing waiting time t_w after the end of the evaporation process. However we did not find any significant change of the $g(r)$ and MSD up to $t_w = 300\, t_B$.

A similar vitrification process was realised in the theoretical NE-SCGLE approach using a compression procedure. The system was initially prepared in a fluid state at a volume fraction $\phi_0 = 0.4$ (note that his is the 3D volume fraction, not the 2D area fraction used in experiments) and temperature $T^* = 0.001$. From this

state the system was brought to a final volume fraction $\phi_f = 0.6$ using five instantaneous compressions of amplitude $\Delta\phi = 0.04$. In each step the system was allowed to relax for a certain time, until reaching ϕ_f after $t_1 = 6t_B$, where t_B is the Brownian time. Once reached ϕ_f, the system was aged for a time $t_2 = 160t_B$. The compression process is indicated in the state diagram of Fig.2a
Fig.2b shows the $g(r)$ obtained for the initial fluid state and the final glass state. The variations of the pair distribution function closely resemble those of the experiments, with an increase of the peak amplitudes with increasing ϕ and a shift of the position to smaller distances, indicating the densification of the system. Similarly, the MSD reported in Fig.2c at ϕ_f shows an extended plateau characteristic of dynamical arrest.

B. Vitrification by Radius Increase at Constant Particle Number Density

An alternative route to vitrification is provided by changes in temperature T, which lead to a change in particle size and thus changes in volume fraction. The sample with $\phi_A = 0.69$ is found in a glass state at T = 25 °C, as discussed in the previous section. Starting from T = 25 °C we increased the temperature of this sample in steps of 1 °C until reaching the temperature of 30 °C. We did not increase T to higher values in order to avoid the occurrence of attractive interactions between particles [50, 51]. At each temperature between 25 and 30 °C we acquired series of 2D images of the sample as soon as the temperature was equilibrated, which took approximately 120s for every 1 °C. After acquiring the data at T = 30 °C the heating devices were switched off and the sample was left to cool down back to 25 °C under the influence of blown air. In this case, the time needed for the sample to decrease its temperature by 1 °C was approximately 300 s. Note that this is a relatively slow process compared with T-quenches presented in previous work on similar systems [28, 32, 34, 35]. We first compare the results obtained for the extreme temperatures, T = 25 °C and 30 °C (Fig.3). The radial distribution function $g(r)$ (Fig.3a), presented as a function of $r/2R$ to take into account the size variation associated with the T change, shows a considerable reduction of the height of the peaks and a shift of their positions to higher values of $r/2R$. This can be understood in terms of the reduction of the area fraction associated with the reduction of the particle size.

The MSD shown in Fig.3b for T = 30 °C is much increased compared to 25 °C and approaches a diffusive behavior. This is consistent with the expected transition to a fluid state associated with the reduction of the volume fraction of the sample indicated by the $g(r)$. Fig.3c shows that the reduction of the height of the first peak of $g(r)$, $g^{\max}(r_1)$, and the shift of its position r_1 to larger values is initially smooth and becomes more pronounced when increasing T above 27 °C. Fig.3d evidences that the MSD, calculated in this case at a specific time $t = 10.56$ s (Δr_0^2), also increases gradually with increasing T, with a T dependence which is compatible with a power-law dependence on T.
When cooling down the system to 25 °C the structure and dynamics show different results compared to the heating up process (Fig.3c,d). The peaks of the $g(r)$ are now smaller (Fig.3c). The MSD is generally larger at all T (Fig.3d). Note that these differences considerably overcome the error bars, which where estimated as the standard deviation of the set of repeated measurements for the peak of $g(r)$, and as the maximum deviation fro the average for the MSD. We observe therefore a hysteresis, leading to a less pronounced structural arrangement of the particles and faster dynamics. Note that the equilibration time in the cooling down process is slightly longer, indicating that the observed effects cannot be attributed to equilibration effects. At 25 °C the MSD still indicates dynamical arrest (not shown): however, the localization length corresponding to the height of the plateau of the MSD is larger (Fig.3d). This suggests that after the initial melting, a different, looser glass state reforms through the T variation route. It should be noted that the aging of this glass state is shorter than the one formed through the particle number density route. Indeed we already mentioned that the original state at T = 25 °C presents an aging time $t_a \sim 10^4 t_B$. On the other hand, the glass formed by decreasing the temperature from the melted state at T = 30 °C, and measured as soon as the temperature equilibrates, presents an aging $t_m \sim 10^1 t_B$.

In the NE-SCGLE theory calculations the heating and cooling processes were realised in the following way: starting from the aged state at $\phi = 0.60$ and $T_i^* = 0.001$, the temperature was increased in five steps of $\Delta T^* \approx 0.2$ until reaching $T_f^* = 1.0$. For each step the sample was left equilibrating for a time $\Delta t = 6t_B$. After reaching T_f^*, the system was cooled down to $T_i^* = 0.001$ again in five steps of equal duration and amplitude. Figs.4a,b show the comparison of the $g(r)$ and MSD in the initial aged glass state and in the state reached after heating up the system to $T_f^* = 1.0$. In agreement with the experimental results we observe the melting of the glass, resulting in a $g(r)$ with smaller peaks which resembles that of the initial fluid sample at $\phi = 0.4$, and an MSD which is characteristic of diffusive behaviour.

Fig.4c shows the T^*-dependence of the height of the first peak of $g(r)$ during the heating and successive cooling process. During the heating process the peak height reduces, as already shown in Fig.4a. When cooling down the system to $T^* = 0.001$, the peak heights increase again. The values at high temperatures are equal to those obtained when heating up the sample, however at the two smallest T^* the values are smaller than along the heating process. In the MSDs calculated at a finite time $t = 10$ (Fig.4d) one can observe that along the cooling process the values at the two smallest T^* are larger, indicating a larger mobility of the particles. Both observations are in

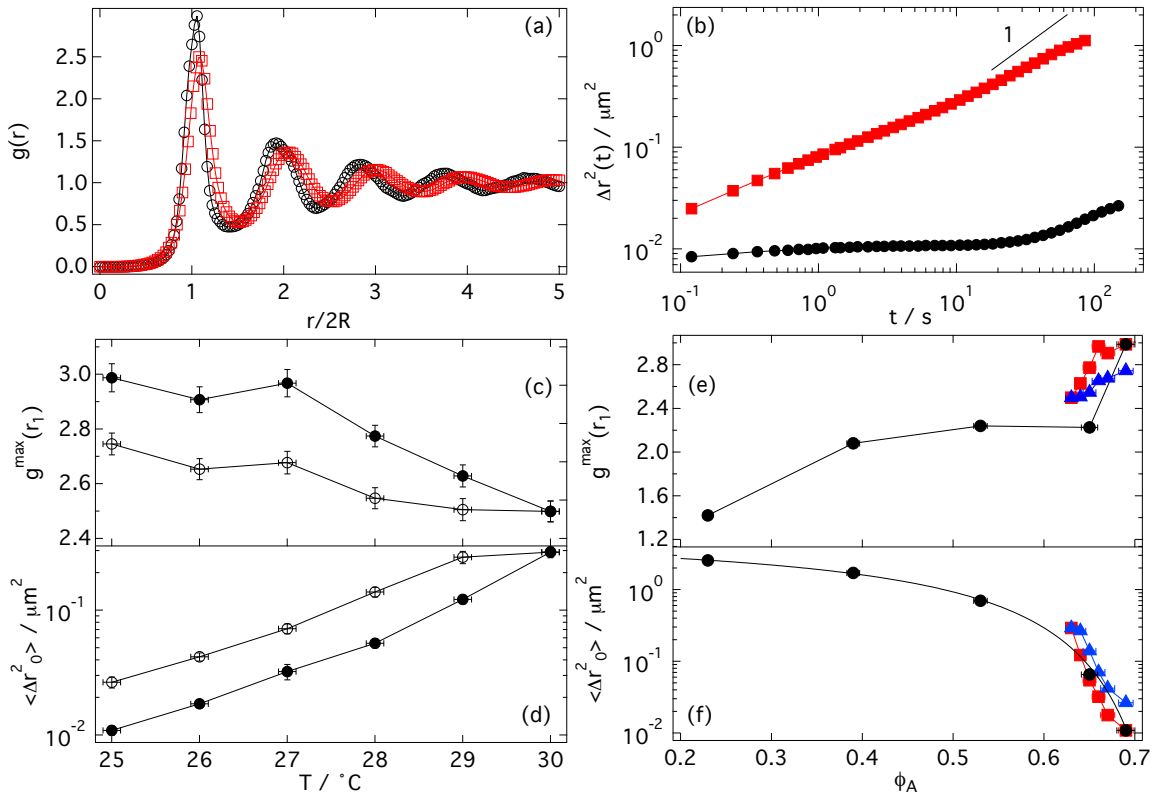

FIG. 3. (a) Radial distribution function $g(r)$ and (b) Mean square displacement obtained from experiments, for $\phi_A = 0.69$ at T = 25 °C (circles) and 30 °C (squares).Temperature dependence of: (c) Height $g^{\max}(r_1)$ of the first peak of $g(r)$ (d) MSD value at $t = 10.56$ s, Δr_0^2. Full symbols: Data collected heating up the sample from 25 to 30 °C. Open Symbols: Data collected cooling down the sample from 30 to 25 °C. (e) Value of the first peak of $g(r)$, $g^{\max}(r_1)$ and (f) MSD value at $t = 10.56$ s, $\langle\Delta r_0^2\rangle$ as a function of the area fraction ϕ_A, for the constant temperature (T = 25 °C) route (circles), and the temperature variation route, when increasing (squares) and decreasing (triangles) the temperature T. Black line in b) is a fit to a VFT dependence of $\langle\Delta r_0^2\rangle$ on ϕ_A. Vertical error bars are in most cases smaller than the symbol size.

good qualitative agreement with the experiments in the region of small T^*, and indicate that after the cooling process the initial, aged glass state is not recovered. The theory helps us elucidating this result looking in more detail at the time-evolution of the MSD calculated at $t = 10$, $\langle\Delta r_0^2\rangle$, along the heating and cooling process (Fig.5). During the steps of the heating process $\langle\Delta r_0^2\rangle$ decreases: along the first step a steady-state value is not achieved, while this occurs after some time in the successive steps. This is because the long aging of the initial state at $T^* = 0.001$ does not allow to reach a steady-state at $T^* = 0.2$ in the heating process. In the first four steps of the cooling process a steady-state is also achieved, however, in the last step this is not. The question whether a state comparable to the initial state will be reached at long aging times will be answered in the following section. The fact that we observe an hysteresis in Figs. 3 and 4 is thus associated to the fact that the final state after cooling is not a steady state of the system. In this sense the hysteresis will thus vary with the time at which we observe the cooled state, i.e. with the aging of this state.

We can observe that the differences in the experimental data at different temperatures are more pronounced than in the theoretical data. This might be an effect of the shorter aging of the initial state in the theory ($t_2 \sim 10^2 t_B$) compared to the experiments ($t_a \sim 10^4 t_B$). We therefore realised an additional initial theoretical state with $t_2 \sim 10^3 t_B$ (longer waiting times could not be reached in a reasonable computational time) and repeated the heating and cooling processes. The results reported in Figs.4c,d show that for the heating process the difference of the values of the radial distribution function and MSD along the heating and cooling processes increase, and the difference extends to higher effective temperatures $T^* = 0.4$. Note that this can be associated to the fact that during the heating process the state barely evolves during the equilibration time in the temperature range $0.001 \leq T^* \leq 0.4$ (Fig.5). It is also important to note that the cooling process does not change, since it starts from the same fluid state at $T^* = 1.0$. Therefore we can conclude that the difference in the degree of hys-

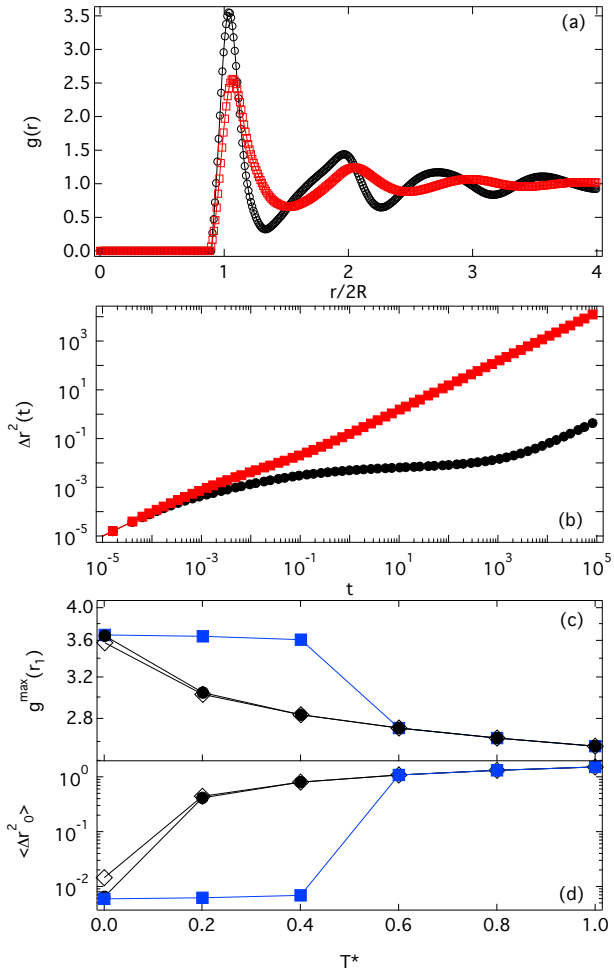

FIG. 4. (a) Radial distribution function $g(r)$ and (b) Mean square displacement obtained from NE-SCGLE theory, for $\phi = 0.6$ and $T^* = 0.001$ (circles) and 1.0 (squares).Temperature dependence of: (c) Height $g^{\max}(r_1)$ of the first peak of $g(r)$ (d) MSD value at $t = 10$, $\langle \Delta r_0^2 \rangle$. Full Circles: Data for an initial aging $t_2 = 160 t_B$ collected heating up the sample from $T^* = 0.001$ to 1.0. Open Diamonds: Data collected cooling down the sample from $T^* = 1.0$ (final state of full circles) to 0.001. Full squares: corresponding data for an initial aging $t_2 = 1500 t_B$.

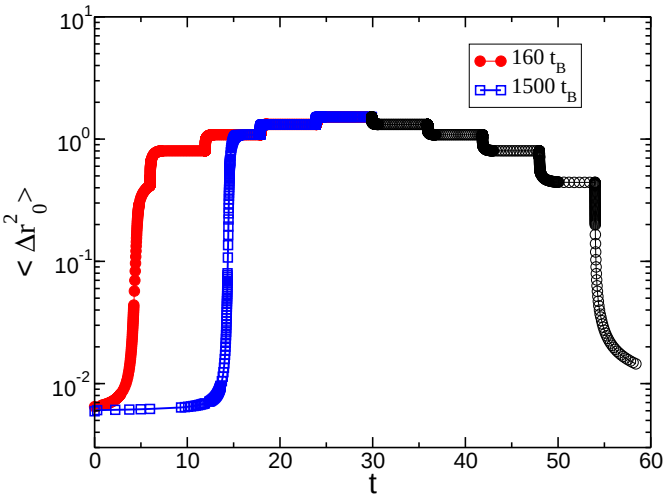

FIG. 5. Time evolution of the mean square displacement obtained from NE-SCGLE theory calculated at $t = 10$, $\langle \Delta r_0^2 \rangle$, along the heating and cooling process. Full red circles correspond to the heating process and open black circles to the cooling process with an aging of the initial state obtained by compression $t_2 = 160 t_B$. Full blue squares correspond to the heating process of the system with an initial aging $t_2 = 1500 t_B$.

teresis observed in the theory and experiments can be attributed to the aging of the initial sample.

C. Comparison of the Particle Number Density and Radius Increase Routes

We compare for the experiments the two routes to the glass state presented in the previous section in more detail. We report in Fig.3e,f the values of the height of the first peak of $g(r)$, $g^{\max}(r_1)$, as well as the values of the MSD calculated at a specific time $t = 10.56$ s, $\langle \Delta r_0^2 \rangle$, as a function of the area fraction ϕ_A for the two different routes. The T variation route spans a relatively small range of area fractions due to the limitation to temperatures $T \leq 30$ °C. As already commented at higher T the particle-particle interaction would change significantly. It is to mention that the initial state of the T variation route is the same state as the end state of the constant T route. The data of the particle number density route show for the peak of $g(r)$, $g^{\max}(r_1)$, a pronounced increase at small ϕ_A which then tends to plateau around $\phi_A = 0.60$ and then suddenly increases again at $\phi_A = 0.69$. The values of Δr_0^2 show a pronounced decrease with increasing ϕ_A which is compatible with a Vogel-Fulcher-Tamman (VFT) dependence of the kind $\langle \Delta r_0^2 \rangle = \Delta r_{00}^2 \exp[-B/(\phi_A^0 - \phi_A)]$ [20]. A fit to this functional dependence gives a value of $\phi_A^0 = 0.78$, which could be taken as an estimate of the critical area fraction for the glass transition. In the radius increase route, when melting the glass from the state at $\phi_A = 0.69$ the values of $g^{\max}(r_1)$ show a significant difference compared to the constant T route, at comparable values of ϕ_A. In particular $g^{\max}(r_1)$ is larger than along the particle number density route. This suggests that the melting process obtained by the T-induced size variation of the particles leads to slightly more ordered samples. The dynamics represented by $\langle \Delta r_0^2 \rangle$ initially seem to follow the same trend as the particle number density route, however start to deviate considerably at around $\phi_A = 0.65$, showing more pronounced displacements. This suggests a faster transition to the fluid state compared to the particle number density route. When reforming the glass by decreasing T, as already discussed in the previous section the changes in $g^{\max}(r_1)$ are more moderate with increas-

ing ϕ_A and the peak at $\phi_A = 0.69$ is smaller than in the particle number density route. As already discussed, this does not seem to be an effect of the different aging of the system, since the difference persists at longer aging times. We rather think that the higher disorder in the glass formed by the T variation route might be a result of freezing the structural correlation of the liquid into the glass through the swelling process. The faster T-induced variation of the area fraction might lead to dynamical frustration that induces only a partial rearrangement of the structural organization of the fluid state. In addition it is possible that changes in the degree of charging of the system with temperature also affect the glass obtained via the temperature variation route [42], and that aspects of jamming physics start to affect solidification through temperature jumps [26, 29]. The dynamics show even more pronounced displacements than in the melting process and are more pronounced for $\phi_A = 0.69$ compared to the particle number density route. However, as discussed in the previous section, this appears to be an aging effect and the dynamics at longer waiting times approach those of the sample obtained by the particle number density route. The ϕ_A dependence of the dynamics along the T-variation route could not be tested against any functional dependence due to the limited range of values of ϕ_A.

D. Aging of the Glass formed through the radius increase route

We monitored the aging behavior of the final glass state obtained along the radius increase route. For this sample we determined the radial distribution function $g(r)$ and the MSD for different waiting times t_w after the temperature was stabilized. The results for $g(r)$ reported in Figs.6a,c show an interesting and unexpected behavior: initially the first peak increases with increasing t_w. However, after 5.4 10^3 s we observe that it starts to slightly decrease, suggesting the onset of structural rejuvenation. At the same time the peak position r_1 increases from the value $r_1 = 2R$ for $t_w = 0$ to $r_1 = 2.05R$ for $t_w > 0$, as seen in the inset of Fig.6a. The observed changes are moderate, but reproducible. It should be also noticed that we did not observe any significant change in the image quality at long waiting times, which could affect the determination of $g(r)$. We see therefore that instead of approaching the value of the peak of the glass formed through the particle number density route, the height of the first peak of the sample formed through the radius increase route diverges from that value. The fact that the position and height of the first peak of $g(r)$ initially increase for $t_w > 0$ possibly indicates a small swelling of the particles. At later aging times the peak height reduces, while the position remains constant (inset of Fig.6). This might indicate that the small swelling of the particles initially leads to a moderate increase of the inter-particle distance and an increase of contacts, followed eventually by rearrangements which relax the structure to a configuration comparable to the initial one, but keeping the slightly larger average inter-particle distance. The origin of the swelling might be related to a small temperature decrease along the aging measurement. Theoretical calculations (Fig.6e) indicate instead a monotonic behavior in which a small increase of the peak height of the $g(r)$ is observed with increasing waiting time and at long aging time the value of the peak obtained through the particle number density route is reached. The effect of the specific choice of the interaction potential on this trend should be investigated in the future. The corresponding MSDs from experiments (Fig.6d) and theory (Fig.6f) show a progressive slowing down of the dynamics, a behavior typical of glasses which has been observed previously [32, 34, 35, 52]. We can see that at the longest waiting time the value of the MSD is very close to the one of the glass state obtained through the particle number density route. This indicates that from the point of view of the dynamics, the two glass states become comparable if the glass state formed through the radius increase route is given sufficient time to age.

E. Second Melting and Vitrification in the radius increase Route

After the first cycle of T-induced shear-melting and vitrification described in the previous section, we repeated the process for an additional cycle. We therefore induced melting of the glass formed through the T-variation route and successively reduced the temperature to again vitrify the sample, following the same route as in the previous cycle. This time we did not measure the structure and dynamics at all intermediate temperatures, only at T = 27.5 °C (on top of T = 25 and 30 °C). When increasing T we observe again the reduction of the area fraction in the $g(r)$, i.e. the peaks decrease and move to larger distances (Fig.7a). Also the dynamics become faster, as shown by the increase of the MSD (Fig.7b). When the sample is cooled down to 25 °C the peaks of $g(r)$ increase again and move to shorter distances, i.e. ϕ_A increases again (Fig.7a). The MSD shows dynamical arrest, as evidenced by an extended plateau (Fig.7b). The difference with the first cycle can be found when comparing the $g(r)$ and the MSD of the glasses at 25 °C, before the melting and after cooling down and vitrifying the sample again. This time the differences in the $g(r)$ and MSD are much more moderate (Fig.7a,b), also at intermediate temperatures, as shown by the values of the height of the first peak of $g(r)$ and $\langle \Delta r_0^2 \rangle$ shown in the insets of Fig.7. This might be associated to the fact that now the glass is formed through the same protocol. Moreover the two glass states present a comparable degree of aging. We should notice that a slight difference in the height of the first peak of $g(r)$ is present, however the difference is considerably smaller than when comparing the glasses formed through the particle number density and radius

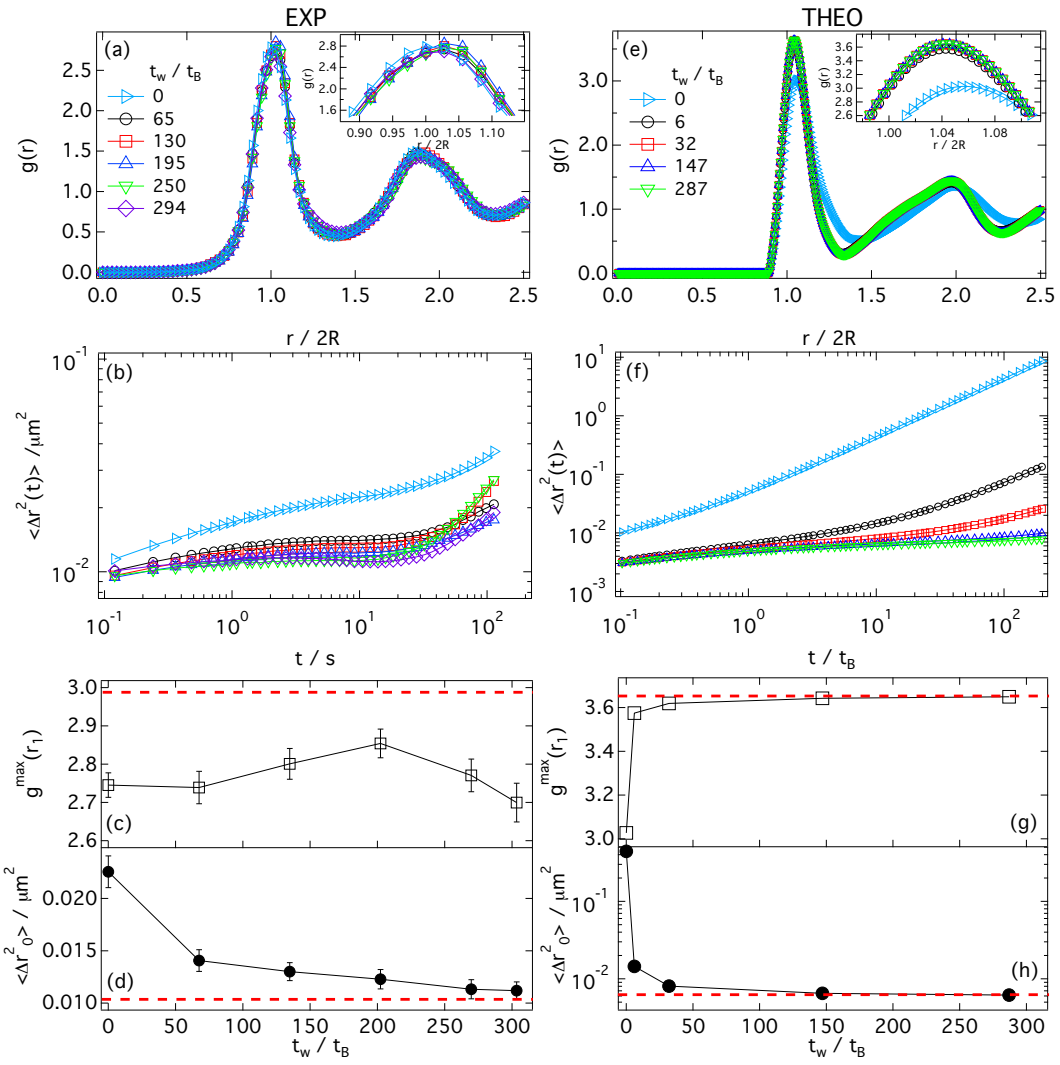

FIG. 6. (a,e) Radial distribution function $g(r)$ and (b,f) Mean square displacement $\langle \Delta r^2(t) \rangle$ of the sample obtained from the first radius increase process from (a,b) experiments ($\phi_A = 0.69$, T = 25 °C) (e,f) theory ($T^* = 0.001$), as a function of aging time t_w (as indicated). Inset of (a,e): Zoom on the first peak of $g(r)$. (c,g) Height $g^{\max}(r_1)$ and (d,h) $\langle \Delta r_0^2 \rangle$ as a function of t_w, extracted from experimental data in (a,b) and theoretical data in (e,f). Dashed red lines: Values of $g^{\max}(r_1)$ and $\langle \Delta r_0^2 \rangle$ for the glass obtained through the particle number density route.

increase routes.

We compare the experimental results with NE-SCGLE calculations, where a similar protocol with two heating and cooling cycles was realised. Fig.8a shows, similar to Fig.7, the radial distribution functions obtained after the first cooling down to $T^* = 0.001$, after the second heating to $T^* = 1.0$, and after the second cooling down to $T^* = 0.001$. We can observe that the $g(r)$ obtained after the second cooling down process is practically identical to the one obtained after the first cooling down process, while the $g(r)$ of the heated up sample indicates a more dilute, fluid structure. The MSDs reported in Fig.8b show a similar result, with the data of the two glassy samples obtained from different cooling down processes essentially indistinguishable. Once more the theory allows us to monitor the time-evolution of the state of the system by means of the non-equilibrium static structure factor (Fig.8c). Comparing the data of the first and second cooling processes one can clearly see that in each ΔT^* step the system reaches the same value. Moreover in the first four steps a steady state condition is achieved, whilst in the last the system is still evolving. However, the non-steady state achieved in the distinct cooling processes is the same, supporting the experimental observation that comparable aging leads to a reproducible non-equilibrium state. These results indicate that the radius variation route is a suitable way of obtaining rejuvenation of glassy PNIPAM dispersions which can be used as an alternative or in combination with shear-induced rejuvenation, which has been discussed in particular detail for

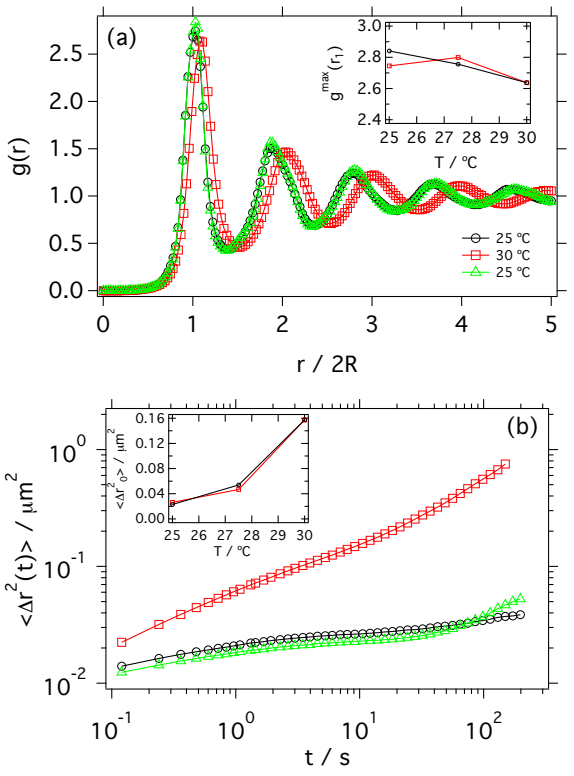

FIG. 7. (a) Radial distribution function $g(r)$ and (b) Mean square displacement $\langle \Delta r^2(t) \rangle$ obtained from experiments for sample with $\phi_A = 0.69$ at different temperatures T (as indicated), within a cycle of melting and vitrification. Insets: (a) Height $g^{\max}(r_1)$ and (b) $\langle \Delta r^2(t = 10.26s) \rangle$ as a function of T, during the heating up (squares) and cooling down (circles) processes.

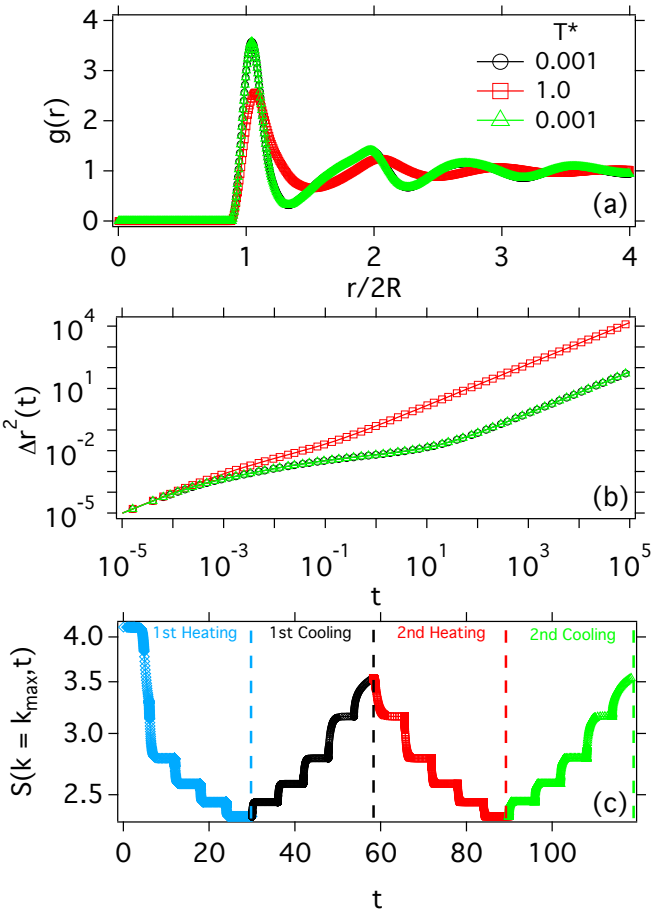

FIG. 8. (a) Radial distribution function $g(r)$ and (b) Mean square displacement $\langle \Delta r^2(t) \rangle$ obtained from NE-SCGLE theory for the sample with $\phi = 0.60$ and different temperatures T (as indicated), within a cycle of melting and vitrification. (c) Height of the first peak of the non-equilibrium structure factor $S(k = k_{\max}, t)$ as a function of time, calculated during the two cycles of heating up and cooling down processes (as indicated).

hard sphere-like colloids [53–57]. It should be noted that while the properties of the glass after rejuvenation are typically controlled by the shear-rate or oscillation frequency in shear-induced rejuvenation, in this case the T-variation rate might be the control parameter and should be investigated in future studies.

IV. CONCLUSIONS

We compared arrested states obtained from dispersions of thermo-sensitive PNIPAM particles following distinct routes: an increase of the volume fraction by radius change at constant particle number density, or a change of the particle number density at constant radius. We realised qualitatively similar protocols in NE-SCGLE theoretical calculations. Experiments and theory show a good qualitative agreement, supporting the interpretation of solidification in terms of the glass transition. Our results indicate that the glass state obtained through the radius increase and the particle number density route are comparable, in terms of dynamics, at sufficiently long aging times, despite the significantly different non-equilibrium routes that lead to glass formation. However, in the experiments the two glasses show structural differences which persist even at long aging times. We speculate that these structural differences might arise from the substantially different processes that lead to glass formation: in the particle number density route, the structure is progressively rearranging to accommodate the increasingly higher number of particles; instead in the temperature variation route the structure of the fluid is quenched into the glass and the particles are limited in their rearrangements due to dynamical frustration induced by the sudden swelling. Further investigation needs to clarify why the dynamics are less affected by these effects. At short aging times, the glass formed along the radius increase route increasingly differs from that obtained along the number density route when the aging of this last state is larger. This arises from the fact that the glass state

obtained through the radius increase route is unaffected by the aging of the system before melting. We find in addition that the radius increase route leads to a reproducible glass state when applied consecutively to the sample. This route results therefore particularly suited for rejuvenating the sample, for example in rheological experiments, without the need of pre-shearing. Future work should investigate possible contributions to solidification related to the jamming scenario [23, 26].

V. ACKNOWLEDGMENTS

This work was supported by the Consejo Nacional de Ciencia y Tecnología (CONACYT, México) through Grants: 242364, 182132, FC-2015-2-1155, Cátedras CONACyT-1631, Laboratorio Nacional de Ingeniería de la Materia Fuera de Equilibrio-279887-2017 and CB-2015-01-257636.

[1] A. Fernandez-Nieves, H. Wyss, J. Mattsson and D. Weitz, *Microgel Suspensions: Fundamentals and Applications*, Wiley, 2011.
[2] W. McPhee, K. C. Tam and R. Pelton, *J. Colloid Interface Sci.*, 1993, **156**, 24 – 30.
[3] K. S. Oh, J. S. Oh, H. S. Choi and Y. C. Bae, *Macromolecules*, 1998, **31**, 7328–7335.
[4] B. Sierra-Martín, Y. Choi, M. S. Romero-Cano, T. Cosgrove, B. Vincent and A. Fernández-Barbero, *Macromolecules*, 2005, **38**, 10782–10787.
[5] S. M. Hashmi and E. R. Dufresne, *Soft Matter*, 2009, **5**, 3682–3688.
[6] T. Lowe, J. Virtanen and H. Tenhu, *Polymer*, 1999, **40**, 2595–2603.
[7] M. R. Islam, Y. Gao, X. Li and M. J. Serpe, *J. Mater. Chem. B*, 2014, **2**, 2444–2451.
[8] J. Kim, M. J. Serpe and L. A. Lyon, *J. Am. Chem. Soc.*, 2004, **126**, 9512–9513.
[9] P. J. Yunker, K. Chen, M. D. Gratale, M. A. Lohr, T. Still and A. G. Yodh, *Rep. Prog. Phys.*, 2014, **77**, 056601.
[10] A. M. Alsayed, M. F. Islam, J. Zhang, P. J. Collings and A. G. Yodh, *Science*, 2005, **309**, 1207–1210.
[11] Z. Wang, F. Wang, Y. Peng, Z. Zheng and Y. Han, *Science*, 2012, **338**, 87–90.
[12] Y. Han, N. Y. Ha, A. M. Alsayed and A. G. Yodh, *Phys. Rev. E*, 2008, **77**, 041406.
[13] Y. Peng, Z. Wang, A. M. Alsayed, A. G. Yodh and Y. Han, *Phys. Rev. Lett.*, 2010, **104**, 205703.
[14] Y. Han, Y. Shokef, A. M. Alsayed, P. Yunker, T. C. Lubensky and A. G. Yodh, *Nature*, 2008, **456**, 898–903.
[15] R. Borrega, M. Cloitre, I. Betremieux, B. Ernst and L. Leibler, *Europhys. Lett.*, 1999, **47**, 729.
[16] H. Senff and W. Richtering, *J. Chem. Phys.*, 1999, **111**, 1705–1711.
[17] Purnomo, E. H., van den Ende, D., Mellema, J. and Mugele, F., *Europhys. Lett.*, 2006, **76**, 74–80.
[18] M. Fuchs and M. Ballauff, *J. Chem. Phys.*, 2005, **122**, 094707.
[19] J. Mattsson, H. M. Wyss, A. Fernandez-Nieves, K. Miyazaki, Z. Hu, D. R. Reichman and D. A. Weitz, *Nature*, 2009, **462**, 83–86.
[20] X. Di, K. Z. Win, G. B. McKenna, T. Narita, F. m. c. Lequeux, S. R. Pullela and Z. Cheng, *Phys. Rev. Lett.*, 2011, **106**, 095701.
[21] N. Koumakis, A. Pamvouxoglou, A. S. Poulos and G. Petekidis, *Soft Matter*, 2012, **8**, 4271–4284.
[22] A. Ikeda, L. Berthier and P. Sollich, *Phys. Rev. Lett.*, 2012, **109**, 018301.
[23] A. Ikeda, L. Berthier and P. Sollich, *Soft Matter*, 2013, **9**, 7669–7683.
[24] K. van der Vaart, Y. Rahmani, R. Zargar, Z. Hu, D. Bonn and P. Schall, *J. Rheol.*, 2013, **57**, 1195–1209.
[25] A. J. Liu and S. R. Nagel, *Nature*, 1998, **396**, 21.
[26] K. N. Nordstrom, E. Verneuil, P. E. Arratia, A. Basu, Z. Zhang, A. G. Yodh, J. P. Gollub and D. J. Durian, *Phys. Rev. Lett.*, 2010, **105**, 175701.
[27] Z. Zhang, N. Xu, D. T. N. Chen, P. Yunker, A. M. Alsayed, K. B. Aptowicz, P. Habdas, A. J. Liu, S. R. Nagel and A. G. Yodh, *Nature*, 2009, **459**, 230–233.
[28] D. Paloli, P. S. Mohanty, J. J. Crassous, E. Zaccarelli and P. Schurtenberger, *Soft Matter*, 2013, **9**, 3000–3004.
[29] A. Basu, Y. Xu, T. Still, P. E. Arratia, Z. Zhang, K. N. Nordstrom, J. M. Rieser, J. P. Gollub, D. J. Durian and A. G. Yodh, *Soft Matter*, 2014, **10**, 3027–3035.
[30] L. Berthier and T. A. Witten, *Phys. Rev. E*, 2009, **80**, 021502.
[31] A.-M. Philippe, D. Truzzolillo, J. Galvan-Myoshi, P. Dieudonné-George, V. Trappe, L. Berthier and L. Cipelletti, *arxiv:1712.02634v1*, 2018.
[32] X. Peng and G. B. McKenna, *Phys. Rev. E*, 2014, **90**, 050301.
[33] P. Yunker, Z. Zhang, K. B. Aptowicz and A. G. Yodh, *Phys. Rev. Lett.*, 2009, **103**, 115701.
[34] R. Colin, A. M. Alsayed, J.-C. Castaing, R. Goyal, L. Hough and B. Abou, *Soft Matter*, 2011, **7**, 4504–4514.
[35] Q. Li, X. Peng and G. B. McKenna, *Soft Matter*, 2017, **13**, 1396–1404.
[36] J. J. Crassous, M. Ballauff, M. Drechsler, J. Schmidt and Y. Talmon, *Langmuir*, 2006, **22**, 2403–2406.
[37] M. Ledesma-Motolinía, M. Braibanti, L. F. Rojas-Ochoa and C. Haro-Pérez, *Colloids Surf., A*, 2015, **482**, 724 – 727.
[38] L. A. Fernández, V. Martín-Mayor and P. Verrocchio, *Phys. Rev. Lett.*, 2007, **98**, 085702.
[39] N. B. Wilding and P. Sollich, *J. Chem. Phys.*, 2010, **133**, 224102.
[40] E. Zaccarelli, C. Valeriani, E. Sanz, W. C. K. Poon, M. E. Cates and P. N. Pusey, *Phys. Rev. Lett.*, 2009, **103**, 135704.
[41] T. Still, K. Chen, A. M. Alsayed, K. B. Aptowicz and A. Yodh, *J. Colloid Interface Sci.*, 2013, **405**, 96 – 102.
[42] M. Braibanti, C. Haro-Pérez, M. Quesada-Pérez, L. F. Rojas-Ochoa and V. Trappe, *Phys. Rev. E*, 2016, **94**,

032601.
[43] J. C. Crocker and D. G. Grier, *J. Colloid Interface Sci.*, 1996, **179**, 298 – 310.
[44] P. Ramírez-González and M. Medina-Noyola, *Phys. Rev. E*, 2010, **82**, 061503.
[45] P. Ramírez-González and M. Medina-Noyola, *Phys. Rev. E*, 2010, **82**, 061504.
[46] R. Juárez-Maldonado, M. A. Chávez-Rojo, P. E. Ramírez-González, L. Yeomans-Reyna and M. Medina-Noyola, *Phys. Rev. E*, 2007, **76**, 062502.
[47] H. C. Andersen, J. D. Weeks and D. Chandler, *Phys. Rev. A*, 1971, **4**, 1597–1607.
[48] *Theory of Simple Liquids*, ed. J.-P. Hansen, and I. R. McDonald, Academic Press, Oxford, Fourth Edition edn., 2013.
[49] G. Brambilla, D. El Masri, M. Pierno, L. Berthier, L. Cipelletti, G. Petekidis and A. B. Schofield, *Phys. Rev. Lett.*, 2009, **102**, 085703.
[50] G. Romeo, A. Fernandez-Nieves, H. M. Wyss, D. Acierno and D. A. Weitz, *Adv. Mater.*, 2010, **22**, 3441–3445.
[51] H. Wang, X. Wu, Z. Zhu, C. S. Liu and Z. Zhang, *J. Chem. Phys.*, 2014, **140**, 024908.
[52] R. E. Courtland and E. R. Weeks, *J. Phys.: Condens. Matt.*, 2003, **15**, S359.
[53] V. Viasnoff and F. m. c. Lequeux, *Phys. Rev. Lett.*, 2002, **89**, 065701.
[54] D. Bonn, S. Tanase, B. Abou, H. Tanaka and J. Meunier, *Phys. Rev. Lett.*, 2002, **89**, 015701.
[55] A. S. Negi and C. O. Osuji, *J. Rheol.*, 2010, **54**, 943–958.
[56] S. A. Rogers, P. T. Callaghan, G. Petekidis and D. Vlassopoulos, *J. Rheol.*, 2010, **54**, 133–158.
[57] M. Ballauff, J. M. Brader, S. U. Egelhaaf, M. Fuchs, J. Horbach, N. Koumakis, M. Krüger, M. Laurati, K. J. Mutch, G. Petekidis, M. Siebenbürger, T. Voigtmann and J. Zausch, *Phys. Rev. Lett.*, 2013, **110**, 215701.